Detection of pigment network in dermoscopy images

Ana Catarina Fidalgo Barata - ISR/IST
Jorge Salvador Marques - ISR/IST
Jorge de Mariz Rozeira - Hospital Pedro Hispano

November 27, 2011

Abstract

Pigment network plays a major role in skin lesion classification and in melanoma detection. Recently, some automatic systems for the detection of this differential structure have been proposed. However, most of these works do not extract the shape of pigment network, which is of major importance in the analyses of dermoscopy images by dermatologists. The work developed proposes a new method for pigment network detection and extraction based on its color and geometry. A new method for lesion classification regarding the presence of pigment network is also proposed. The algorithm achieves a $SE = 78\%$ and a $SP = 77\%$ for lesion classification, in a dataset of 57 dermoscopy images from the dermoscopy service of Hospital Pedro Hispano - Matosinhos. [1]

Keywords: Skin lesion classification, Dermoscopy, Melanoma, Pigment Network detection, Directional Filters, Connected Component Analysis, Features Extraction

1 Introduction

Melanoma is one of the deadliest forms of cancer, being responsible for most of the deaths related with skin cancer. However, when detected in an early stage it can be cured by recurring to a simple excision [1]. Therefore, it is important to develop methodologies that allow a premature and correct detection of melanomas.

Dermoscopy is a non-invasive screening technique used by dermatologists to visualize skin lesions. By recurring to this technique dermatologists are able to amplify the lesion by a factor of 6x-100x. With the magnification, pigmented structures that can not be seen by the naked eye become visible [1]. These structures can then be used by experts to classify the lesion (melanocytic or not) and evaluate if it is malignant (melanoma) or not, by recurring to one of the several methods proposed by clinicians to diagnose a skin lesion (*e.g.* ABCD rule [26], 7-point check-list [3] and Menzies method [22]). It has been proved by Mayer *et al.* [21] that dermoscopy can improve the accuracy of melanoma detection by 10-27% when used by a well trained dermatologist. However, the diagnosis of a skin lesion by one of the previous medical methodologies is a subjective one, since it depends on human vision, lacking reproducibility. Moreover, its accuracy is highly dependent on the expertise of the dermatologist [8].

Computerized dermoscopy image analyses systems (CAD systems) do not have the limitation of subjectivity. These consider that a computer can a second independent diagnose tool, which can be used by non-experienced operators to perform a preliminary evaluation of a clinical case. They can also be used to improve biopsy decision-making and follow-up [17]. Several systems for lesion classification, and ultimately for melanoma detection, have been proposed by different groups [9, 19, 23]. These systems usually start by performing an automatic segmentation of the lesion, followed by a process of feature extraction which describe color, texture and shape, and finally a lesion classification using learning methods. Some systems have an intermediary step between feature extraction and classification, in which they reduce the size of the

[1] This work was supported by FCT in the scope of project PTDC/SAU- BEB/103471/2008

feature space by eliminating redundant, irrelevant or noisy features.

Despite the promising results, CAD systems have some issues. First of all they do not try to incorporate the medical knowledge. They are based on a machine learning paradigm: if features are rich enough and if there is a (very) large database of lesions classified by experts, inference methods will be able to learn the classification rule [11]. Another problem is related with comparison between different methods, since each groups uses a different dataset it is not possible to determine which system gives actually the best results.

In recent years, automatics systems which try to detect medical features such as asymmetry, border, color and differential structures (dots, pigment network and blue-white veil) have been proposed [2, 7, 10, 12, 13, 16, 24, 25].By detecting these kind of features it is possible to incorporate detailed medical knowledge in the CAD systems.

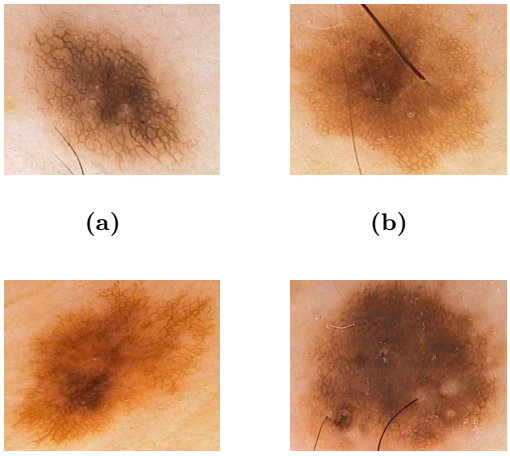

Figure 1: Examples of Pigment Network

Pigment network (see Figure 1) is one of the most important structures in dermoscopy [4]. It appears as a grid of thin brown lines over a diffuse light brown background, having a shape very similar to a honeycomb [1], that can cover the entire lesion or only parts of it. Pigment network is considered the dermoscopic hallmark of benign acquired melanocytic nevi and of thin melanomas because this pattern is related with presence of melanin (protein produce by melanocyts) in the deep layers of the skin. Nevertheless pigment network can also be found in other kind of skin lesions as seborrheic keratosis and dermatofibromas [1]. The assessment of its shape is very important for dermatologists, since pigment network can have a typical or atypical structure, and an atypical pigment network is usually an unmistakable sign of melanoma.

Despite its importance, pigment network was ignored in literature for a long time. Recently, automatic algorithms for pigment network detection have been proposed [2,7,13,16,24]. However, most of them only try to detect the presence of pigment network, without extracting its structure, which is very important for dermatologists. Fleming *et al.* [13] propose an automatic algorithm for extracting and measuring the pigment network characteristics such as its thickness and the size of the holes. They use morphological techniques and their results are purely qualitative. Grana *et al.* [16] propose a similar algorithm for network detection. In their work they try to distinguish lesions which contain pigment network between *complete network* and *partial network* regarding the spatial distribution of pigment network within the lesion. They achieve an overall network detection performance of 88.3%.

Anantha *et al.* [2] propose two algorithms for detecting pigment network in skin lesions. The first one uses a statistics over neighboring gray level dependence matrices and the second one involves filtering with Law energy masks. Their algorithm achieves an accuracy of 80%.

Betta *et al.* [7] algorithm distinguishes between typical and atypical pigment network. To detect the presence of pigment network in a given lesion they combine structural and spectral information. They start by taking the difference of an image and its response to a median filter. This process is followed by a thresholding step and a morphological closing operation. The mask obtained is then combined with a mask obtained using a Fourier analysis and a final mask which highlights pigment network regions is presented. They appear to achieve a $SE = 50\%$ and a $SP = 100\%$.

Sadeghi *et al.* [24] propose and algorithm for pigment network detection based on its color and spatial organization. They start by filtering the image with a LoG filter. The next step is to convert the binary mask obtained into a graph. The detection of pig-

ment network regions is then performed by using the Iterative Loop Counting Algorithm. Their algorithm achieves an accuracy of 94.3% in a dataset of 500 images.

The algorithm described in this paper performs the detection of pigment network regions in dermoscopy images based on its color and geometry, by using a bank of directional filters and a connected component analysis. The algorithm is also capable of extracting the lines of pigment network, which are very important to dermatologists. This does not happen with most of the detection algorithms found in literature, being [13,16] the only two exceptions. The system described is also capable of classify a skin lesion regarding the presence of absence of pigment network. The paper is organized as follows. Section 2 presents an overview of the proposed system. Sections 3 to 7 present the several steps of the algorithm. Section 8 describes an experimental evaluation of the methods and section 9 concludes the paper. Most of this work was published on the main conference on IEEE Biomedical Engineering Society:

C. Barata, J.S. Marques and J. Rozeira [5] - "Detecting the pigment network in dermoscopy images: a directional approach" - in proceedings of the 33rd Annual International Conference of the IEEE Engineering in Medicine and Biology Society (August 30th-September 3rd) at Boston (USA) .

2 System Overview

Fig. 1 shows several examples of lesions in which pigment network is present. By inspecting the different images it is possible to conclude that pigment network may exhibit different visual characteristics, namely color, width and spacial distribution. However, the main properties of pigment network (dark grid lines over a lighter diffuse background and the organization of these connected lines that lead to the existence of holes) are always present and can be used to its detection. Section 3 and 5 explain how these two properties are used to perform the detection of pigment network.

Dermoscopy images might present some artifacts, such as hair or reflection produced during the acquisition process, that bring additional difficulties to the detection problem. These artifacts must be removed before trying to detect the network. The removal of these artifacts is performed in a pre-processing step described in Section 4.

An additional validation of the network regions obtained can be performed by using a patter recognition approach. This additional step is required since the network detection block tends to detect regions in excess. The procedure used is described in Section 6.

The lesion classification step is the final block of the system. The classification is a binary labeling of a lesion as *with* or *without pigment network*. This algorithm will be described in Section 7.

Figure 2 summarizes the detection system briefly described above.

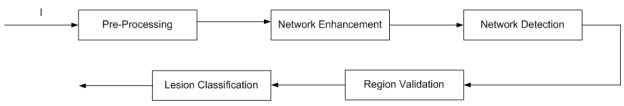

Figure 2: Block Diagram of the Detection System

3 Directional Filters

Two of the structures to be detected in this work (pigment network and hair artifacts) contain linear strokes, with highly directional shapes. Therefore, filters which are able to detect features in a specific direction, called directional filters, can be used to enhance them. To design these filters two principles were used: the human perception of vision and the definition of receptive fields [18] and the processing of signals with noise [27]. Based on these two principles it was possible to design a directional filters bank with an impulse response similar to the one that describes the functioning of the receptive fields [20] and that matched the shape of the structures to be detected [27]. The functioning of the directional filters bank is shown in Fig. 3.

The analysis bank is composed of several directional filters each of them tuned to a specific orientation $\theta_i \in [0, \pi], i = 0...N$. The filters were designed this way because the linear structures that compose the artifacts and the network not only have an unknown direction but may appear in a dermoscopy image with more than one orientation as well.

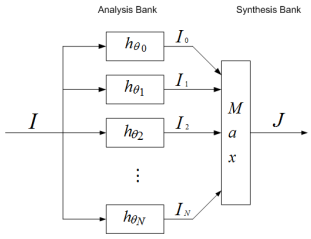

Figure 3: Directional Filters Bank. The inpute I and all the outputs I_i are images

Each one of the filters from the analysis block has the impulse response

$$h_{\theta_i}(x,y) = G_1(x,y) - G_2(x,y) \tag{1}$$

where G_k is a Gaussian filter:

$$G_k(x,y) = C_k \exp\{-\frac{x'^2}{2\sigma_{x_k}^2} - \frac{y'^2}{2\sigma_{y_k}^2}\}, k = 1,2 \tag{2}$$

In (2) C_k is a normalization constant and the values of (x', y') are related with (x, y) by a rotation of amplitude θ_i

$$x' = x\cos\theta_i + y\sin\theta_i \tag{3a}$$

$$y' = y\cos\theta_i - x\sin\theta_i \tag{3b}$$

The values for the parameters σ_{x_k} and σ_{y_k} are chosen in such a way that the second filter is highly directional and the first one is less directional or even isotropic. A difference of gaussians was chosen since this design allows a better enhancement of directional structures while removing the effect of the background. The image I is decomposed in $N+1$ filtered images I_i by using all the directional filters

$$I_i = h_{\theta_i} * I \tag{4}$$

The outputs of the $N+1$ are then combined as follows. To synthesize the final image J a simple maximization is performed at each pixel

$$J(x,y) = \max_i I_i(x,y) \tag{5}$$

4 Pre-Processing

The pre-processing algorithm performs two key operations: hair detection and reflection detection. It is important to detect and remove these structures before applying the pigment network detection block, since both of them can occlude part of the network to be detected.

The dermoscopy images used are *rgb* images stored in *bitmap* and *jpeg* formats. Before performing the artifacts detection the images are converted in gray scale ones by choosing the highest entropy channel as follows

$$S(i) = -\sum_{k=0}^{L-1} h_i(k)\log[h_i(k)] \tag{6}$$

where $h_i(k)$ is the histogram of the color component i and $L = 256$ bins, since each color channel ranges from $0, ..., 255$.

4.1 Reflection Detection

Reflections appear in dermoscopy images as a result of the presence of air bubbles in the immersion oil at the interface between the skin and the face plate of the dermatoscope or other acquisition system. The algorithm proposed for reflection detection is very simple. By inspecting the intensity profile of the images used was possible to determine that pixels which belong to regions classified as reflection have higher values of intensity than other pixels in the same image and that those values diverge substantially from the average intensity I_{avg} computed in their neighborhood. Therefore, to be classified as reflection a pixel (x, y) should meet the following condition

$$I(x,y) > T_{R1} \wedge I(x,y) - I_{avg}(x,y) > T_{R2} \tag{7}$$

where I is the gray scale image, I_{avg} is the average intensity in a local neighborhood of the pixel and T_{r1}, T_{r2} are both threshold values. Fig. 4 shows an example of the reflection detection algorithm.

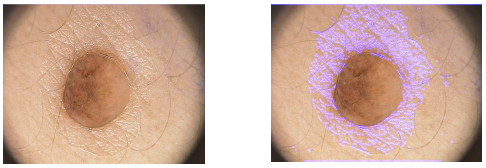

(a) Original **(b)** Output

Figure 4: Reflection detection

4.2 Hair Detection

Hair artifacts are highly directional structures with a linear shape. Usually they have a coloration much darker than the background (skin or lesion), but that is not always the case. The algorithm proposed

for hair detecting uses a bank of directional filters (1 - 5) to filter the gray scale image I. After, a binary classification of all the pixels from the filters response J is performed by enforcing the following condition

$$J(x, y) > T_H \tag{8}$$

where T_H is a threshold value determined empirically. A pixel (x, y) is classified as hair if it is above T_H. Fig.5 shows an examples the hair detection algorithm.

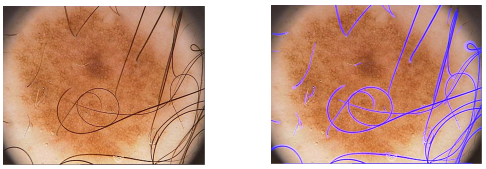

(a) Original **(b)** Output

Figure 5: Hair detection

4.3 Image Inpaiting

The artifacts detected are removed by multiplying the gray level image by a binary mask which combines the output of the two artifacts detection systems. The resulting gaps are then filled by applying a PDE-based interpolating algorithm called image inpaiting [6]. This algorithm uses the information of the neighborhood to fulfill the unknown regions. By applying this removal step it is possible to minimize the influence of artifacts and avoid false alarms, i.e., the detection of not pigment network regions.

5 Network Detection

The dark lines of pigment network are ones of its most common characteristics. These lines are highly directional linear structures which are enhanced by directional filters (1 - 5). The bank of directional filters used to perform enhancement of pigment network lines is similar to the one used for hair detection. However, the filter parameters ($\sigma_{x_k}, \sigma_{y_k}$ and N) are different since the length of each line stroke in the pigment network is much smaller than the case of the hair artifacts. The output of the filters bank is compared with a threshold T_N as in (8). The two steps described are part of the network enhancement block. Next, the network detection block will be described.

The network detection block takes into account the geometry of pigment network. It is assumed that pigment network is a set of connected regions. Therefore, by performing a 8-connectivity connected component analysis over the binary image obtained after the first two steps, the connected dark lines can be extracted. Of all the connected regions detected only the ones which have areas are bigger than a threshold are selected as being part of the pigment network. Let R_i be the $i-th$ connected region. The area criteria that the region must fulfill is

$$A(R_i) > A_{min} \tag{9}$$

where $A(R_i)$ denotes the area of the region R_i and A_{min} is the threshold. By enforcing this conditions it is possible to exclude connected components with small areas.

6 Region Validation

The network detection algorithm proposed previously detects regions in excess, which means that it detects most of all the pigment network regions in a dataset but has many false alarms too. The detection algorithm is a simple one, which does not explore all pigment network properties. Therefore, some region post-processing can be done to improve the detection results. A pattern recognition approach will be adopted. First, features will be extracted from each of regions detected. These features characterize each one of the regions regarding their intensity, texture and topology and will be then used to train a classifier (AdaBoost [28]) to distinguish pigment network regions from not pigment network regions.

Before performing the region validation step the background of each one of the regions detected is added to the output of the network detection block, which consists only of the mesh of pigment network. This is done by using morphological operations.

6.1 Feature Extraction

The vector of features extracted from each region is composed of features which describe texture, intensity and geometry or shape (area of the network, number of holes, etc). The total number of features is 51 and they can be divided in two different groups:

Image Features - comprise information about intensity (histogram of intensities, variance) and texture (histogram of gradient (HoG), entropy), leading to a total of 38 features. The histogram of intensities uses 26 bins, which leads to a total of 26 features. Variance and entropy are computed using the commonly know formulas [14,15], corresponding each one to a single feature. The HoG of an image $I(x,y)$ is computed as follows

$$hog_i = \sum_{(x,y)\in I(x,y)} G(x,y)\cdot b_i(\theta(x,y)) \tag{10}$$

where $G(x,y)$ is the amplitude of the gradient of $I(x,y)$, $\theta(x,y)$ is the phase and

$$b_i(\theta(x,y)) = \begin{cases} 1 & \text{if } \theta \in i\text{-th bin} \\ 0 & \text{if otherwise} \end{cases} \tag{11}$$

10 bins, with an angular interval of 18°, are used so computing the HoG leads to 10 features.

Topological Features - try to separately characterize the structure of the network and holes. The structure of the network is characterized by two features: network area and network area after erosion, obtained after applying a morphological erosion to the output of the network detection block. The holes and their shape are characterized by 11 features: number of holes and histogram of the area of holes (10 bins, i.e., 10 features).

All the features are normalized by using the area of the region.

6.2 Classification

The algorithm used to learn the classification function was the AdaBoost [28] which classifies the data using an ensemble C_T of simple classifiers denoted as weak classifiers. This algorithm was chosen not only because it gives good results in challenging objects recognition problems, e.g.face detection, but also because this algorithm is able to select a good subset of informative features for a given problem (feature selection). This subset is selected by assuming that each classification function depends on a single feature. The classifier was trained in order to determine the best set of parameters T number of iterations, best feature vector x_k and α, which is a weight initialization parameter used as follows

$$w_k = \begin{cases} \frac{\alpha}{m} & \text{if } y_k = 1 \\ \frac{1}{l} & \text{if } y_k = 0 \end{cases} \tag{12}$$

where m is the number of positive examples (*pigment network*- label $y_k = 1$) and l is the number of negative examples (*not pigment network* - label $y_k = 0$).

7 Lesion Classification

Pigment network is usually a structure regularly meshed with narrow spaces, which is distributed more or less regularly throughout the lesion [1]. This suggests that pigment network is a dense structure. Assuming this, an algorithm that classifies a lesion based on an area ratio is proposed to classify lesions as *with* or *without pigment network*. To perform the area ratio it is necessary to segment the skin lesion. The dermoscopy images are manually segmented and a binary mask S_{GT} is obtained for each one of them.

The statistics computed is the following

$$\lambda = \frac{A(R)}{A(S_{GT})} \tag{13}$$

where $A(S_{GT})$ is the area of the segmentation and $A(R)$ is the area of the region defined as follows

$$R = [\bigcup_{i:A(R_i)>A_{min}\wedge C_T(R_i=1)} R_i] \cap S_{GT} \tag{14}$$

R is the union of all the detected and validated regions within a lesion. Therefore, R can be defined as the final pigment network region and is only composed of the potential skeleton of pigment network, the "holes" are not considered. The classification of a lesion L is performed in the following way

$$L = \begin{cases} \textit{with pigment network} & \text{if } \lambda \geq T_A \\ \textit{without pigment network} & \text{if } \lambda < T_A \end{cases} \tag{15}$$

where T_A is a threshold empirically determined.

8 Results

The proposed algorithm was tested in a dataset of 57 dermoscopy images, extracted from the database of Hospital Pedro Hispano - Matosinhos. This set contains RGB images of size around 576x767, stored in *bitmap* and *jpeg* formats. Each color component is in

the range 0, ..., 255. The images were acquired during clinical exams using a dermatoscope and a magnification of 20x. The set contained 13 images with pigment network.

For each image a ground truth was constructed by the author under the guidance of an expert. Each image was classified regarding the presence of pigment network (denoted as lesion ground truth). In the cases where pigment network was present, the pigment network regions were manually segmented. This manual segmentation is called region ground truth G_T (see Figs. 6(a) and 6(b)). For training the classifier a label was given to each region detected by the network detection block (see Fig 6(c)). Since there were regions partially occupied by pigment network, it was decided that the labeling process should be done by imposing two threshold conditions. Only regions containing more than 70% of the pigment network area , when compared with the region ground truth, were considered as *pigment network* (label 1), whereas other regions with less than 30% of the pigment network area were considered as *not pigment network* (label 0). Regions with pigment network areas comprised in the interval 30%-70% were discarded (see Fig. 6(d)).

The dataset used was small. Therefore, a K fold cross validation procedure ($K = 5$) was adopted to perform the evaluations, i.e., the total number of images was divided into five subsets (folds) so that each one of them contained approximately the same number of positive and negative examples. Four of them were used for training and the fifth was used for testing. This procedure was repeated five times so that each subset was used once for testing.

Three different algorithms were evaluated: the region detection algorithm, the classifier and the lesion classification algorithm. The performance was assessed through the computation of the following probabilities:

(1) Assessment of Region Detection: uses a region matching procedure in which the binary output of the detection system B_N is compared with the region ground truth G_T. Each detected region can be classified as: Correct detection (CD) if the detected region matches one or more regions in G_T, False Alarm (FA) if the detected region has no correspondence or Detection Failure (DF) if one ground truth region has no correspondence. The region matching algorithm works as follows. Considering that G_T is composed of P regions and that B_N contains M detected regions, a correspondence matrix C is defined by

$$C(i,j) = \begin{cases} 1 & \text{if } A(B_{N_j} \cap G_{T_i}) \geq 0.3A(B_{N_j}) \\ & \qquad \forall\, i \in \{1,\ldots,\mathrm{P}\}, j \in \{1,\ldots,\mathrm{M}\} \\ 0 & \text{if otherwise} \end{cases} \tag{16}$$

where $A(B_{N_j} \cap G_{T_i})$ is the area of the region $B_{N_j} \cap G_{T_i}$ and $A(B_{N_j})$ is the area of B_{N_j}. Two auxiliary vectors are also defined

$$L(i) = \sum_{j=1}^{P} C(i,j) \quad i \in 1,\ldots,M \tag{17}$$

$$K(j) = \sum_{i=1}^{M} C(i,j) \quad j \in 1,\ldots,P \tag{18}$$

A region B_{N_j} is classified as CD if $K(j) \geq 1$. This ensures that detected regions which are actually the merge of two regions of the ground truth are only accounted once as CD. Detected regions which result from a split of a ground truth region are independently classified as CD. FA and DF are determined by computing the number of empty columns or lines in C, respectively.

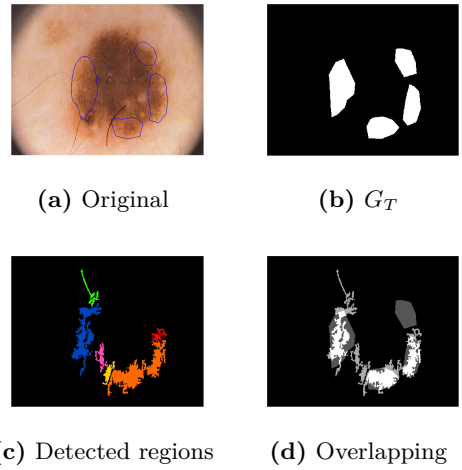

(a) Original **(b)** G_T **(c)** Detected regions **(d)** Overlapping

Figure 6: Overlapping with G_T:A(blue) = 74% (label 1), B(green) = 0% (label 0), C(pink) = 0% (label 0), D(yellow) = 0% (label 0), E(orange) = 76% (label 1), F(red) = 24% (label 0).

(2) Assessment of the Validation Step: it is performed by computing the values of sensitivity SE

and specificity SP as follows

$$SE = \frac{\#TP}{\#TP + \#FN} \tag{19a}$$

$$SP = \frac{\#TN}{\#TN + \#FP} \tag{19b}$$

where $\#TP$ stands for the number of true positive regions, $\#FP$ is the number of false positive regions, $\#TN$ is the number of true negative regions and $\#FN$ is the number of false negative regions.

(3) Assessment of Lesion Classification: it is performed by computing SE and SP as in (19). In this case $\#TP$ stands for the number of true positive lesions, $\#FP$ is the number of false positive lesions, $\#TN$ is the number of true negative lesions and $\#FN$ is the number of false negative lesions.

The classifier was trained with different values for $\alpha \in \{1, 3, 5, 10, 15\}$, different combination of features (only image features, only topological features and both) and different number of iterations T. The overall performances obtained for the complete set of images are synthesized in Tables 1 and 2

Table 1: Statistical Results for the different α values and $T = 2000$. FP-rate stands for the percentage of not pigment network regions that are wrongly classified ; TP-rate is the percentage of correctly classified pigment network regions.

	Image Features		Topological Features		Both	
α	FP-rate	TP-rate	FP-rate	TP-rate	FP-rate	TP-rate
1	22%	30%	20%	44%	18%	38%
3	26%	35%	21%	45%	22%	42%
5	27%	36%	24%	45%	23%	42%
10	29%	37%	24%	46%	24%	45%
15	30%	39%	25%	47%	26%	45%

In Table 1 FP-rate is equal to $100\% - SP$ and TP-rate is equal to SE. By inspecting the table it is possible to conclude that the best value for α is 15 and the features which better discriminate between pigment network and not-pigment network regions are the topological ones, since higher values of TP-rate and lower values of FP-rate are achieved with them. Nevertheless, the TP-rate is a low value. This value can be increased by reducing the number of iterations, as can be seen in Table 2. $T = 2000$ was used to determine the α value and the best features vector because it guaranteed that there were no errors in the training set. This might have led to an overfitting of the classifier to the training data, which explains the results obtained.

Table 2: Statistical results for different numbers of iterations for $\alpha = 15$ and topological features. FP-rate stands for the percentage of non-network regions that are wrongly classified as so while TP-rate is the percentage of correctly classified pigment network regions.

T	FP-rate	TP-rate
100	49%	86%
150	46%	77%
200	45%	75%
300	40%	74%
2000	25%	47%

By inspecting Table 2 it is possible to determine that the best value for the number of iterations is $T = 100$. Using $\alpha = 15$, $T = 100$ and topological features the classifier achieves a $SE = 86\%$ and a $SP = 51\%$.

The output of the detection system is illustrated in Fig 7. The algorithm achieves good detection results in all of the examples, despite the different characteristics of the pattern.

Fig.8 shows two examples of detection errors. One is caused by the presence of a strong circular texture called cobblestone pattern (see 8(a)), in which the algorithm detects the boundaries of the circular structures. The second detection error is caused by the presence of a dots pattern (see 8(c)).

Table 3 shows the overall performance of the region detection algorithm before and after the validation step.

Table 3: Statistical results for the network detection system before and after the validation step. The validation is performed with $\alpha = 15, T = 100$ and topological features. CD - correct detection; FA - false alarm; DF - detection failure.

	Before Validation	After Validation
CD	15	13
FA	53	27
DF	1	3

By inspecting the number of FA and DF before the validation step it is possible to confirm that in fact the detection block detects regions in excess, which leads to a low number of DF but a high number of FA too. After the validation step, the number o FA reduces considerably, which suggests that the validation step brings benefits to the detection system. The number of CD decreases slightly. This is expected since the SE of the classifier is not equal to 100% for the best

parameters (see Table 2, $T = 100$).

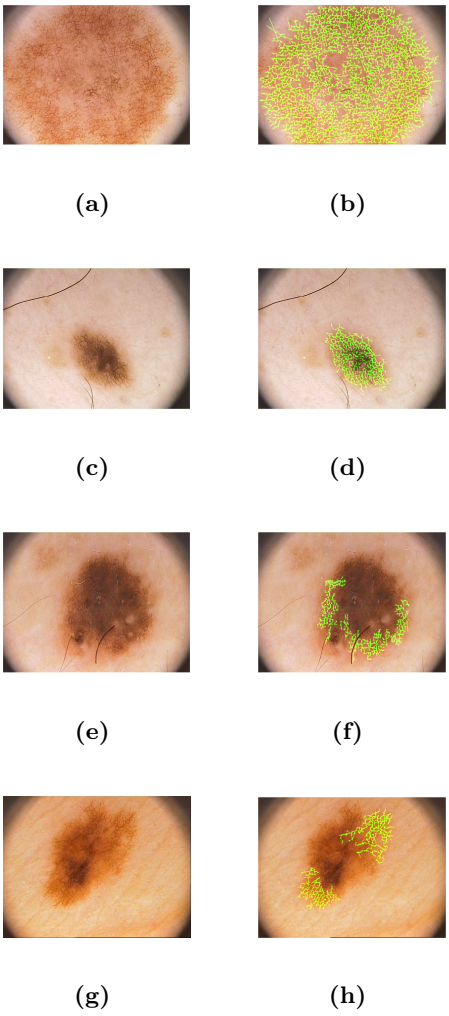

Figure 7: Output of the automatic detection system for lesions with Pigment Network: original image (left), pigment network detection(right)

Table 4 shows the overall performance of the lesion classification algorithm before and after the validation step. It is possible to see that the SP of the algorithm increases around 14% with the validation step. The decrease in the SE after the validation can be explained by two different facts: first, the increase of DF after the validation, which represents a decrease in the number of regions used to perform the statistics based classification (see Section 7) and second, the lesion classification before the validation step uses all the detected regions, even the ones which will be discarded during the region labelling process. Nevertheless, the results obtained for lesion classification and region detection prove that the validation step is an important one.

Table 4: Statistical results for the lesion classification algorithm before and after the validation step. The validation is performed with $\alpha = 15, T = 100$ and topological features. SE - sensitivity; SP - specificity.

	Before Validation	After Validation
SE	85%	78%
SP	63%	77%

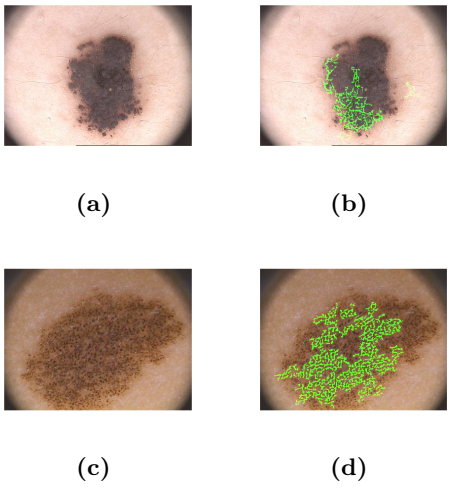

Figure 8: Output of the automatic detection system for lesions without Pigment Network: original image (left), detection errors(right)

9 Conclusions

This paper describes an automatic algorithm for pigment network detection and lesion classification. The detection is performed by exploring the color and geometrical properties of pigment network, using a bank of directional filters and a connected component analysis.

The algorithm achieves good detection scores in a set of images from the database of Hospital Pedro Hispano , for both region detection ($CD = 13$, $FA = 27$ and $DF = 3$) and lesion classification ($SE = 78\%$ and $SP = 77\%$). Therefore, this algorithm is an useful tool in a dermoscopy analysis system.

Future work should rely on testing this algorithm in a larger dataset, trying different vector features combinations (e.g. include features which characterize color) and other learning algorithms. The output of the algorithm can also be used to discriminate be-

tween typical and atypical network, which could increase the medical value of the algorithm.

10 Acknowledgment

The author would like to thank to Prof. Jorge Marques and Dr. Jorge Rozeira for all their support, guidance and help during this thesis. The author would also like to thank to Profs. Teresa Mendonça, André Marçal and Ms. Bárbara Amorim from the University of Porto, Drs. Ofelia Morais, Marta Pereira, Marta Teixeira and nurse Lina Santos from Hospital Pedro Hispano, for their support during this work.

References

[1] Dermoscopy tutorial. http://www.dermoscopy.org/atlas/base.htm.

[2] M. Anantha and *et al.* Detection of pigment network in dermatoscopy images using texture analysis. *Computarized Medical Imaging and Graphics*, 28(5):225–234, 2004.

[3] G. Argenziano and *et al.* Epiluminescence microscopy for the diagnosis of doubtful melanocytic skin lesions. comparison of the ABCD rule of dermatoscopy and a new 7-point checklist based on pattern analysis. *Archives of Dermatology*, (134):1563–1570, 1998.

[4] G. Argenziano and *et al.* Dermoscopy of pigmented skin lesions: results of a consensus meeting via the internet. *Journal of American Academy of Dermatology*, 148(5):375–389, 2003.

[5] C. Barata, J.S. Marques, and J. Rozeira. Detecting the pigment network in dermoscopy images: a directional approach. In IEEE, editor, *33rd Annual International Conference on the IEEE EMBS*, pages 5120–5123, September 2011.

[6] M. Bertalmio and *et al.* Image inpainting. *SIGGRAPH*, pages 417–424, 2000.

[7] G. Betta and *et al.* Dermoscopic image-analysis system: estimation of atypical pigment network and atypical vascular pattern. In *International Workshop on Medical Measurement and Applications*, April 2006.

[8] M. Binder and *et al.* Epiluminescence microscopy of small pigmented skin lesions : short-term formal training improves the diagnosis performance of dermatologists. *Journal American Academy of Dermatology*, pages 197–202, 1997.

[9] M. Celebi and *et al.* A methodological approach to the classification of dermoscopy images. *Computerized Medical Imaging and Graphics*, 31:362–373, 2007.

[10] M. Celebi and *et al.* Automatic detection of blue-white veil and related structures in dermoscopy images. *Computerized Medical Imaging and Graphics*, 32:670–677, 2008.

[11] R. Duda and *et al.* *Pattern Classification.* Wiley, 2001.

[12] G. Fabbrocini and *et al.* Epilluminescence image processing for melanocytic skin lesion diagnosis based on 7-point check list: a preliminary discussion on three parameters. *The open dermatology journal*, 4:110–115, 2010.

[13] M. Fleming and *et al.* Techniques for a structural analysis of dermatoscopic imagery. *Computarized Medical Imaging and Graphics*, (5):375–389, 1998.

[14] R. Gonzalez and R. Woods. *Digital Image Processing.* Prentice Hall, 2 edition, 2002.

[15] R. Gonzalez, R. Woods, and S. Eddins. *Digital Image Processing using MATLAB.* Gatesmark Publishing, 2009.

[16] C. Grana and *et al.* Line detection and texture characterization of network patterns. In *In ICPR'06: Proceedings of the 18th International Conference on pattern Recognition*, 2006.

[17] K. Hoffman and *et al.* Diagnostic and neural analysis of skin cancer (DANAOS, a multicentre study for collection and computer-aided analysis of data from pigment skin lesions using digital dermoscopy. *Britain Journal of Dermatology*, 149(4):801–809, 2003.

[18] D.H. Hubel and T. N. Wiesel. Receptive fields, binocular interaction and functional architecture in the cat's visual cortex. *Journal of Physiology*, 160:106–154, 1962.

[19] H. Iyatomi and *et al.* An improved internet-based melanoma screening system with dermatologist-like tumor area extraction algorithm. *Computerized Medical Imaging and Graphics*, 32:566–579, 2008.

[20] J. P. Jone and L. A. Palmer. An evaluation of the two-dimensional gabor filter model of simple receptive fields in cat striate cortex. *Journal of Neurophysiology*, 58(6):1233–1258, 1987.

[21] J. Mayer. Systematic review of the diagnostic accuracy of dermatoscopy in detecting malignant melanoma. *Medical Journal Australia*, (167):206–210, 1997.

[22] S.W. Menzies and *et al.* Frequency and morphologic characteristics of invasive melanomas lacking specific surface microscopic features. *Archives of Dermatology*, (132):1178–1182, 1996.

[23] P. Rubegni and *et al.* Automated diagnosis of pigment skin lesions. *International Journal of Cancer*, 101:576–580, 2002.

[24] M. Sadeghi and *et al.* A novel method for detection of pigment network in dermoscopic imagesusing graphs. *Computerized Medical Imaging and Graphics*, (35):137–143, 2011.

[25] W.V. Stoecker and *et al.* Detection of granularity in dermoscopy images of malignant melanoma using color and texture features. *Computerized Medical Imaging and Graphics*, 35:144–147, 2011.

[26] W. Stolz and *et al.* ABCD rule of dermatoscopy: a new practical method for early recognition of malignant melanoma. *European Journal Dermatology*, (4):521–527, 1994.

[27] H.L. Van Trees. *Detection, Estimation and Modulation Theory.* John Wiley & Sons, Inc., 2001.

[28] P. Viola and M. Jones. Robust real-time face detection. *International Journal of Computer Vision*, 57(2):137–154, 2004.